sustainability

MDPI

Article

The Performance, Combustion and Emissions of Mechanical Supercharging Modifications on a High-Speed Spark Ignition Engine

Gu Luo [1], Nengsong Zhou [1], Zejia Chen [1], Junyou Zhang [2], Fudong Wang [1] and Banglin Deng [1,*]

[1] Naval Architecture and Shipping College, Guangdong Ocean University, Zhanjiang 524088, China
[2] School of Information and Control Engineering, Liaoning Petrochemical University, Fushun 113001, China
* Correspondence: dengbanglin@gdou.edu.cn

Abstract

Currently, high-speed gasoline engines are increasingly focusing on miniaturization and efficiency. Compared with turbocharging, mechanical supercharging is undoubtedly the more suitable technical approach for small, high-speed gasoline engines. To clarify the influence of the proposed supercharging approach on power, thermal efficiency and emissions within a broad range of engine speeds, this study designed two supercharging schemes (with different supercharger/crankshaft transmission ratios), and conducted bench tests comparing with the original engine. The results showed that the boost effect was more pronounced under medium load conditions. At full load, the high-speed supercharging scheme (94.5/86 ratio) on average improved torque by 10.8%, while the low-speed boost mode (86/61 ratio) only took effect after 5500 rpm. But at 60% load, 94.5/86 and 86/61, respectively, improved torque by 24.4% and 11.7%; thermal efficiencies of both supercharging schemes were almost the same and higher than that of the original operation by 0.8%; thus, the specific fuel consumption was reduced, on average, by ~9.5%. After boosting, the ignition phase was delayed due to the knock limit, but the high cylinder temperature promoted the recovery of the combustion rate in the later stage. In terms of emissions, NO_x increased by 28% with the 94.5/86 scheme, while it decreased very slightly with the 86/61 scheme. CO rose by 3.7% under the 94.5/86 scheme, while it almost did not change under the 86/61 scheme operation, and HC increased by 13% and decreased by 21%, respectively, under the high and low boosting schemes. In conclusion, our proposed supercharging approach improved power and thermal efficiency and afforded a compromise emission effect. This study has revealed the performance trade-off rules of different boosting modes, which can provide important theoretical and technical support for the mechanical supercharging modification of high-speed gasoline engines.

Keywords: high-speed engine; mechanical supercharging; efficiency; combustion; emissions

Check for updates

Academic Editors: Cinzia Buratti and Juan J. Hernández

Received: 16 May 2026
Revised: 24 June 2026
Accepted: 25 June 2026
Published: 27 June 2026

Copyright: © 2026 by the authors. Licensee MDPI, Basel, Switzerland. This article is an open access article distributed under the terms and conditions of the Creative Commons Attribution (CC BY) license.

1. Introduction

Nowadays, as the energy crisis evolves and continuous efforts are made to control environmental pollution [1], the development of gasoline engines has been centered around the core goals of "small displacement, high power, and high efficiency" [2], forming a pattern where multiple technological paths are running in parallel. Among them, pressure boost has been a mainstream technology [3], which has been proven to increase the engine's thermal efficiency [4].

As the earliest industrialized boosting solution, mechanical boosting, with its advantageous structure of direct drive by crankshaft, became the core technology for early high-performance power units [5]. It directly drives the compressor by belts or gears from the crankshaft, achieving a boosting response synchronized with the engine speed and avoiding the lagging defect of exhaust gas turbocharging. With the maturity of exhaust energy recovery technology, turbocharging has gradually become mainstream for passenger vehicles due to its advantage of no crankshaft power loss. Subsequently, variable geometry turbochargers (VGTs) and dual-tube systems have been developed to address the lagging issue. Serrano et al. [6] demonstrated that mechanical supercharging decreased specific fuel consumption at low power conditions, while the turbocharged method showed greater advantages at high power conditions due to more adequate exhaust capacity. However, the unique value of mechanical supercharging in terms of instantaneous response and low-speed torque output has kept its research demand in small high-speed SI (spark ignition) engine modifications [7]. And the combined boosting technology will expand its application scope [8], for example, the combination configuration of electrically driven mechanical supercharging and turbocharging [9].

Regardless of the type of boosting technology, the core requirement is to appropriately increase the intake pressure and intake efficiency, thus improving the engine's thermal efficiency [10]. Mechanical supercharging does well in this aspect, and the linearity of power output is highly consistent with that of naturally aspirated engines, significantly improving the transient acceleration performance of high-speed gasoline engines. However, the strong coupling between the compressor and crankshaft also brings limitations: at high speeds, the compressor speed becomes too high, and the driving power consumption accounts for an excessive proportion of total output power, which will weaken the power gain [7]. Thus, in hybrid vehicles, to decouple the motion between the crankshaft and supercharger, an alternative solution is that the supercharger is driven by electricity [11]. But this solution makes the system more complicated. So, the mechanical efficiency of the mechanical supercharging method needs further investigation under a wide speed range. In terms of efficiency and combustion process, moderate intake pressure boost can increase the density of the mixture and intensity of turbulence in the cylinder, accelerate the speed of flame propagation, shorten the combustion duration, and thereby improve the ITE (indicated thermal efficiency) [12]. However, excessive boost will cause the intake temperature to rise significantly, leading to a tendency for detonation and forcing the ignition timing to be delayed, which, instead, results in a loss of thermal efficiency. Some technologies can alleviate this phenomenon, such as cooled EGR (exhaust gas recirculation) [13], improved combustion chamber design [14], valve timing optimization [15], valve lift optimization [16], spark timing adjustment [17] and/or water injection [18]. In the emission aspect, supercharging generally improves combustion and thus decreases HC and CO emissions [19], while higher temperatures brought by supercharging are more prone to generate higher levels of NO_x [20]. But emissions are very complicated and are affected by many factors, such as operating conditions, air/fuel ratio, combustion temperature and its phase [21]. However, the emission results of mechanical supercharging high-speed SI engines are less frequently reported in communication communities.

From the above description regarding the mechanical supercharging modifications on high-speed SI engines, there is still a lack of in-depth understanding. Specifically, for a sport motorcycle, greater power output is the core requirement, but how to balance power, thermal efficiency, and emissions still needs further investigation. This trade-off effect, for mechanical supercharging, is largely decided by the supercharger/crankshaft transmission ratio. Therefore, in the present work, two mechanical supercharging schemes were designed and retrofitted onto a motorcycle engine. For the updated supercharging,

the engine's performance, working process and emissions were experimentally estimated under a wide speed range. Results indicate that the current supercharging solutions slightly improve thermal efficiency, and at a common load (60% throttle opening), reduce brake-specific fuel consumption (BSFC) by about 9.5%, and achieve a compromise emission effect. So, this study is anticipated to provide an important implication for the upgrade of high-speed engines.

2. Experiments

2.1. Tested Engine and Supercharging Reformation

The original engine is a 4-stroke single-cylinder high-speed SI engine (Figure 1a); its characteristics are listed in Table 1. This engine is installed in a sports motorcycle, whose maximum speed is 180 km/h (with 5 gears), and its size is 2035 × 850 × 1150 mm (Length × Width × Height), with a curb weight of 188 kg. In order to enhance power density, a supercharging retrofit was performed. A mechanical supercharger (SprintexS5-150, Sprintex Ltd., Perth, Western Australia, Australia) was driven by a crankshaft through a transmission belt; the system layout is displayed in Figure 1b. And the supercharger's structure and performance (at 1.4 bar outlet pressure) are given in Figure 2 (the performance was provided by the supercharger manufacturer). As can be seen, the highest volumetric efficiency of the compressor is about 90%; the flow rate almost increases linearly along with compressor speed, but the driving power sharply increases at the high-speed stage.

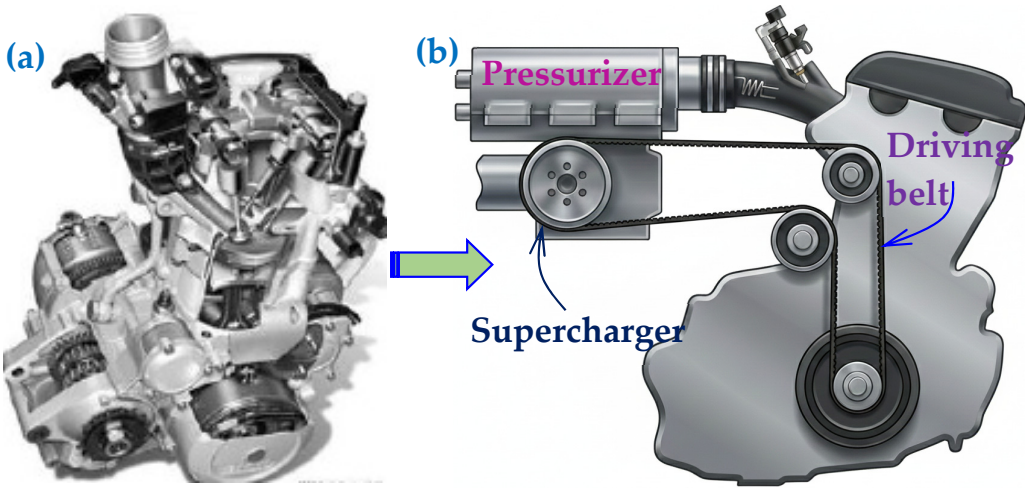


Figure 1. The original engine (**a**) and supercharging engine system layout (**b**).

Table 1. Engine specifications.

Item	Content
Engine type	4 Stroke and single cylinder
Cooling mode	Water cooling
Fuel supply mode	Electronic control port injection
Bore (mm)	100
Stroke (mm)	83
Compression ratio	11.5
Rated power (kW/rpm)	37/6750 (calibration value)
MaxTorque (N·m/rpm)	60/5500 (calibration value)

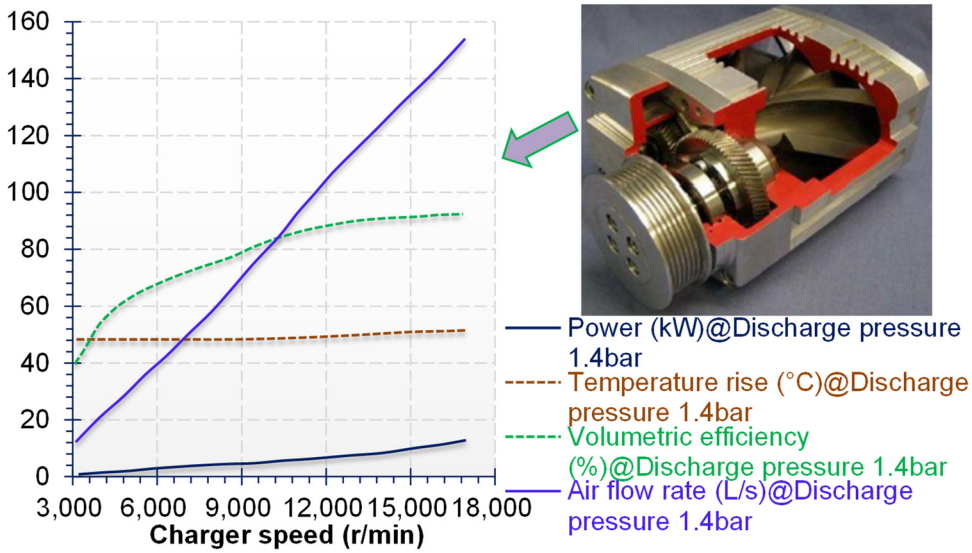


Figure 2. The supercharger structure and its performance characteristics at 1.4 bar discharge pressure.

Then, the transmission ratio was calculated. From the supercharger performance, at a 1.2 pressure ratio, the compressor speed n_c should be larger than 4508 r/min, and extra power is needed to be retained (flow rate leakage and potential sudden acceleration), thus the final pulley diameter ratio (driving side to driven side) was ø94.5/ø86. Of course, to explore the transmission ratio effect, another ratio (ø86/ø61) was added, such that the role of the engine or compressor speed can be investigated. Finally, due to the layout characteristics, some components were simultaneously modified, such as the crankshaft, crankcase cover (output side) and so on.

2.2. Test Condition and Procedure

Firstly, the engine's full-load characteristics were tested to acquire engine performance limits. Then, in order to investigate engine speed effects on engine performance and emissions, the engine was tested under the speed range of 3000–7000 r/min with an interval of 500 r/min (the engine load was kept at 60%), for the original engine and two supercharging schemes. During the whole experiment, the excess air coefficient (λ) was kept constant at 0.85. The ignition advanced angle was set at each condition based on the maximum brake torque (MBT) rule without obvious knock happening; specifically, the KF (knock factor) calculated by Equation (1) should not be larger than 2. And the circumstances and operating conditions of engine tests before and after supercharging should be ensured.

$$KF = \int_{K_0}^{K_0+\Delta\varphi} |p_k| / \int_{K_0-\Delta\varphi}^{K_0} |p_r| \quad (1)$$

where K_0 is the knock crank angle start point that corresponds to the highest pressure of the low-frequency signal; $K_0 + \Delta\varphi$ and $K_0 + \Delta\varphi$ are, respectively, the knock window and reference window; and $|p_k|$ and $|p_r|$ are, respectively, the high-frequency pressure after rectification during the knock window and reference window.

The experimental layout is displayed in Figure 3. The relevant instruments and their characteristic parameters are listed in Table 2. The experimental process was performed based on the national standards of China (GB/T 5363-2008 "Method of Bench Test of Engine for Motorcycles and Mopeds" [22] and GB/T 18297-2024 "Performance test code for road vehicle engines" [23]). And the test procedure was similar to our previous study [24]. Based on an integrated test system and provided instruments, multi-dimensional precise

characterization of power output, combustion process, fuel consumption and emission components was achieved simultaneously. The specific experimental process is as follows:

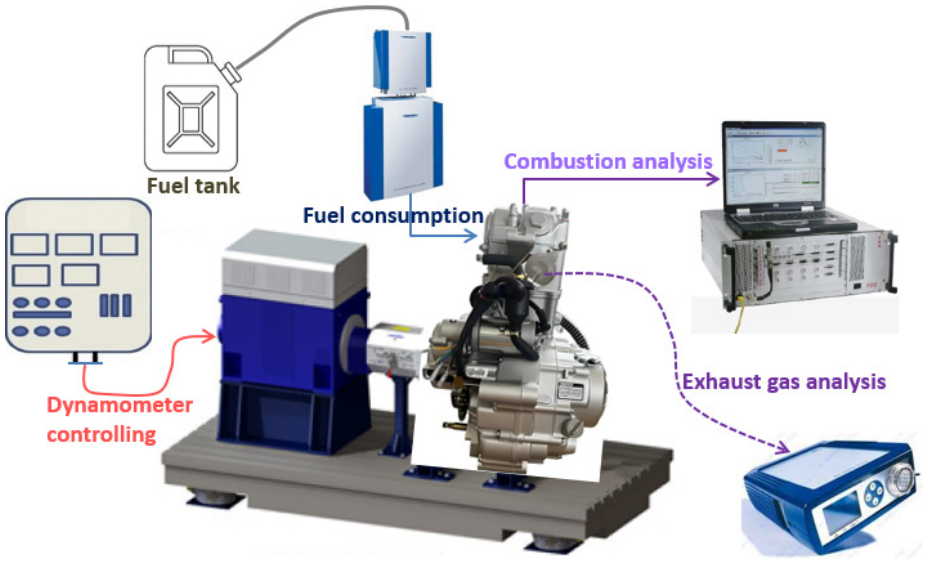


Figure 3. The schematic diagram of the experimental setup.

Table 2. The technical parameters of main test instruments.

Instrument Name	Manufacturer/Type	Measurement Range	Accuracy
Engine dynamometer	100 kW 9157-08-3 (APICOM S.p.A., Ferrara, Italy)	0–100 kW	1 N·m torque, 1% speed
Gas analyzer	AVL/Digas2200 (Xiamen Haiteng Engine Testing Engineering Co., Ltd., Xiamen, China)	CO: 0–10%vol HC: 0–20,000 ppm NO_x: 0–5000 ppm	CO: 0.01%vol HC: 1 ppm NO_x: ±1 ppm
Combustion analyzer	SIRIUSi-HS CA (Dewesoft d.o.o., Trbovlje, Slovenia)	0–200 V	200 ks/s
Intake air conditioning	ACSW3000 (Nanjing JiuDing Refrigeration &Air-conditioning Equipment Co., Ltd., Nanjing, China)	Standard condition: 25 °C, 30% RH, 100 kPa	T: ±1 °C, RH: ±3%, P: ±1 kPa
Air flow meter	DN80 (Beijing Figreth Instrument Co., Ltd., Beijing, China)	0–500 slpm	±1.0%
Fuel consumption meter	CM 082 (APICOM S.p.A., Ferrara, Italy)	0–50 kg/h	±0.10%
Cylinder pressure sensor	6115BFD34Q02 (Kistler Instrumente AG, Winterthur, Switzerland)	0–100 bar	−9.692 bar/v
Intake temperature sensor	Pt 100 (Hanwei Technology Group Co., Ltd., Zhengzhou, China)	−40–+85 °C	±0.15 °C
Coolant/oil temperature sensor	1061B (PCB Piezotronics, Inc., Buffalo, NY, USA)	−40–+200 °C	±0.15 °C
Exhaust temperature sensor	Pt 200 (Hanwei Technology Group Co., Ltd., Zhengzhou, China)	−40–+850 °C	±1.5%

Table 2. *Cont.*

Instrument Name	Manufacturer/Type	Measurement Range	Accuracy
Intake pressure sensor	XTL-190M-500 (Kulite Semiconductor Products, Inc., Leonia, NJ, USA)	0–5 bar	0.2 mV/kPa
Exhaust pressure sensor	EWCTV-312M-17BARA (Kulite Semiconductor Products, Inc., Leonia, NJ, USA)	0–10 bar	266 mV/bar

Before the test, the full system's metrological calibration and preparatory work should be completed first: traceable calibration of the torque and speed sensors of the electric dynamometer should be carried out to ensure the measurement accuracy of the power output parameters; flow calibration of the volumetric fuel consumption meter in series in the fuel supply circuit should be conducted; zero and range calibration of the exhaust gas analyzer should be performed, and the measurement accuracy of the emission components such as CO, HC, and NO_x should be verified using standard gases. The static pressure of the cylinder pressure sensor in the combustion analysis system and simultaneously adjusted the phase accuracy of the crankshaft angle signal should be calibrated. At the same time, the ambient pressure/temperature and relative humidity were measured and recorded to provide basic data for the environmental correction of subsequent parameters.

Then, the test engine was fixed on the base of the test bench through a dedicated fixture. The output end was connected to the dynamometer through a high-precision elastic coupling to eliminate installation misalignment errors. The fuel circuit completed the sealed connection among the fuel tank, fuel consumption meter and engine fuel supply pipe. Meanwhile, the sampling probe of the gas analyzer was connected to the exhaust pipe, and the data acquisition cable was connected to the controller/displayer. The cylinder pressure sensor was installed integrally with the sparking plug, and the crankshaft angle encoder was installed at the front end. The two signals were connected to the combustion analysis acquisition unit. Next, the engine was started and operated at idle conditions for 5 min. Then, gradually the speed was increased to 50% of the rated speed and 50% load for the warm-up process, until the coolant and oil temperature, respectively, stabilized at 85 ± 5 °C and 95 ± 5 °C, eliminating the interference of thermal fluctuations on the test results.

Then, each target operating condition should run stably for more than 30 s. Once the fluctuations of all parameters met the requirements of national standards, the data collection was triggered (the torque was automatically recorded by a dynamometer). The combustion analysis system acquired cylinder pressure and crankshaft angle signals with a resolution of 0.1 °CA (the cylinder pressure was averaged from over 200 cycles), and analyzed core parameters such as heat release pattern and combustion phase; the exhaust analyzer simultaneously collected exhaust components concentrations.

Lastly, the test uncertainty is estimated. The uncertainty was calculated by the Root Sum of Squares (RSSs) of random errors and systematic errors. The former was determined through three repeated trials, while the latter was calculated by the RSSs of all sensor errors involved in a certain result (for example, the measured precision of a species emission involved accuracies of speed, throttle position, exhaust flow rate, gas concentration and so on). Combined with the accuracies of sensors listed in Table 2, the uncertainty of torque, air flow rate, fuel consumption, exhaust temperature and emissions was, respectively, 2.24%, 2.45%, 2.24%, 2.7% and 2.24%. The uncertainty mainly comes from speed and torque control of the dynamometer; the error of other sensors was small, so the overall uncertainties for various results were close and small.

3. Results and Discussion

3.1. Performance and Efficiency

Firstly, Figure 4 gives the engine full load performances and related operating parameters under 3000 r/min to 7000 r/min speed. From Figure 4a, at a low speed of 3000 r/min, the original engine outputted the highest torque, followed by the 94.5/86 supercharging (the compressor speed is higher than the 86/61 mode at a constant engine speed), but this mode outperformed the original machine after 3500 r/min; however, the 86/61 mode requires the speed to exceed 5500 r/min before it can surpass the original machine. In addition, the torque of the original engine showed a significant downward trend after 5500 r/min, while the supercharging models can still maintain a relatively high torque platform in the range of 5500–7000 r/min. Especially for the 94.5/86 transmission ratio scheme, due to the higher speed of the compressor, it provided a more abundant intake air in the high-speed range, effectively alleviating the natural torque attenuation of the engine caused by the decline in charging efficiency (see below). For the combined Figure 4e, the average boosting ratio of the 86/61 supercharging mode was about 1.06; this was not enough to overcome extra resistance before 5500 r/min, while the 94.5/86 supercharging mode improved the average boosting ratio to ~1.19, and achieved a large improvement in power output.

In the aspect of specific fuel consumption, as can be seen in Figure 4b, in the commonly used cruise range of 3500–5500 r/min, the fuel consumption rate of the 94.5/86 supercharging mode was lower than that of the original engine, while the 86/61 mode shortened the low BSFC speed range, and in the acceleration range of 6500–7000 r/min, both supercharging modes lowered the BSFC. This indicates that mechanical supercharging improved combustion efficiency, enabling the engine to reduce fuel consumption per unit of work. However, at 3000 r/min, the BSFC of the supercharging engine was higher than that of the original model. This is because the mechanical supercharger needed to consume a portion of the crankshaft power, and at this time, the mechanical efficiency of the engine was relatively low, resulting in the gain in effective thermal efficiency being partially offset by the mechanical losses. For the thermal parameters, as expected, after supercharging, the intake temperature largely increased, especially for the 94.5/86 model (at the highest temperature, it was almost doubled), as shown in Figure 4c. But from Figure 4d, supercharging merely slightly increased the exhaust temperature (even with the 86/61 mode, the temperature during medium and high-speed reduced); this is because although after supercharging the heat release increased due to more fuel input (the λ was unchanged before and after supercharging), the rise in intake air mass simultaneously consumed more calories for the same temperature rise. Lastly, as displayed in Figure 4f, before 5000 r/min and due to more air mass inspired through supercharging, the unburned mixture temperature may be lower (especially for the 86/61 mode), which was more conducive to suppress auto-ignition, so the spark time can be slightly advanced; however after 5000 r/min, the trend reversed due to in-cylinder heat release, which was largely increased by supercharging (especially for the 94.5/86 mode).

Now, a more frequent condition (60% load) is analyzed. Comparing Figures 4 and 5, similar phenomena were found, but the boosting effect was more pronounced at part load. For example, from Figure 5a, at 3000 r/min, the torque of the supercharging engine was lower than in the original mode. Although the compressor has achieved a positive pressure of 88.8 mbar (94.5/86 mode, see Figure 5e), the power consumed by the crankshaft to drive the compressor was relatively high. Moreover, the intake temperature has risen to 47.8 °C (compared to 33.1 °C in the original machine, Figure 5c), and thus the density compensation effect has not been able to fully counteract the negative effects caused by mechanical losses and the increase in heat load. But after that, the torque enhancement became increasingly

stronger. This was due to a strong boosting effect, as shown in Figure 5e, the 94.5/86 scheme continuously provides a boost pressure of 144–190 mbar above 4000 r/min, effectively compensating for the decrease in charging efficiency caused by the shortened intake time at high speeds (see "Original" results in Figure 6c), thereby maintaining the high torque range. While the boosting effect of the intake pressure of the 86/61 scheme dropped a lot, especially at 6500 r/min, the intake pressure was still higher than the test cell's ambient pressure (0.988 bar). This operating point may encounter the compressor's characteristic dropping point, at which the compressor was working at 4610 r/min and a very slight pressure rise (0.004 bar). This issue will continue to be monitored.

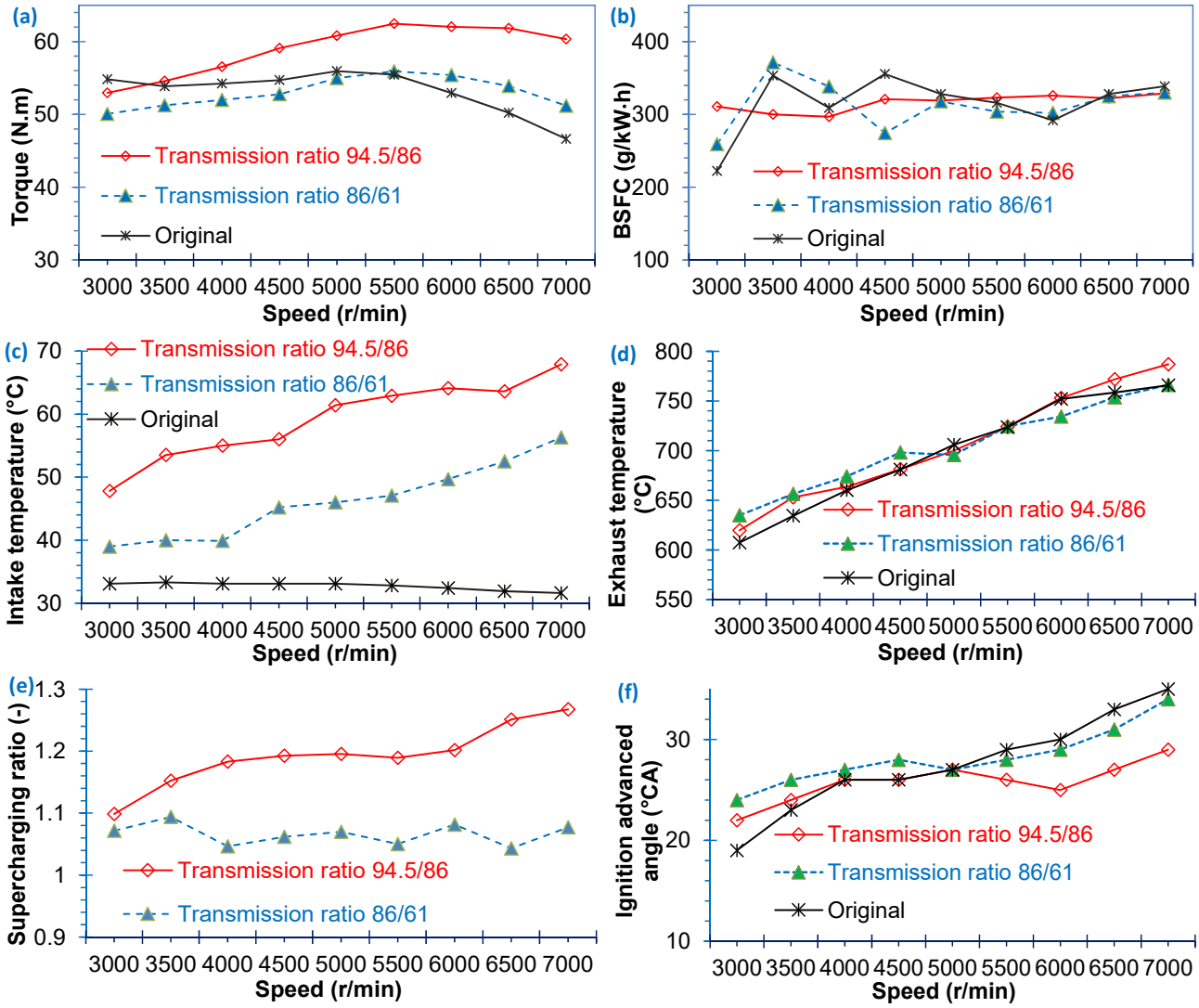


Figure 4. The performances and operating parameters for original and supercharging engine under full load: (**a**) engine torque, (**b**) brake specific fuel consumption, (**c**) intake temperature, (**d**) exhaust temperature, (**e**) supercharging ratio, (**f**) ignition advanced angle.

For the BSFC, as presented in Figure 5b, the high speed supercharging scheme (94.5/86 mode) has achieved a breakthrough improvement in fuel economy: within the core operating range of 4000–6000 r/min, the BSFC has significantly decreased from the original engine's 350–390 g/kWh to the range of 300–310 g/kWh, with a reduction of 15–23%, which was slightly superior to the low speed supercharging scheme (86/61 mode). Although the supercharging schemes required a reduction in the ignition advance angle (for example, advanced angle of 94.5/86 mode retarded from 35 °CA at 6000 r/min to 26 °CA,

see Figure 5f) to avoid too violent combustion, due to the increased intensity of the cylinder internal turbulence and temperature, the combustion duration was shortened, and the isovolumetric degree was increased, which partially compensated for the thermal efficiency loss caused by the delayed ignition. However, there was a "fuel consumption trap" in the low-speed range: the 94.5/86 solution had a BSFC of 310 g/kWh at 3000 r/min, which was much higher than the original engine's 215.4 g/kWh; the 86/61 solution also showed a slight deterioration in fuel consumption at 3000 r/min. As mentioned above, at low speeds, the torque required to drive the compressor accounts for a relatively high proportion of the engine's output torque. At the same time, the increase in intake temperature (after supercharging, the intake air temperature generally increased by 20–30 °C; in the high 94.5/86 scheme, it even reached 66 °C at 7000 r/min, see Figure 5c) led to an increase in heat loss during the compression stroke.

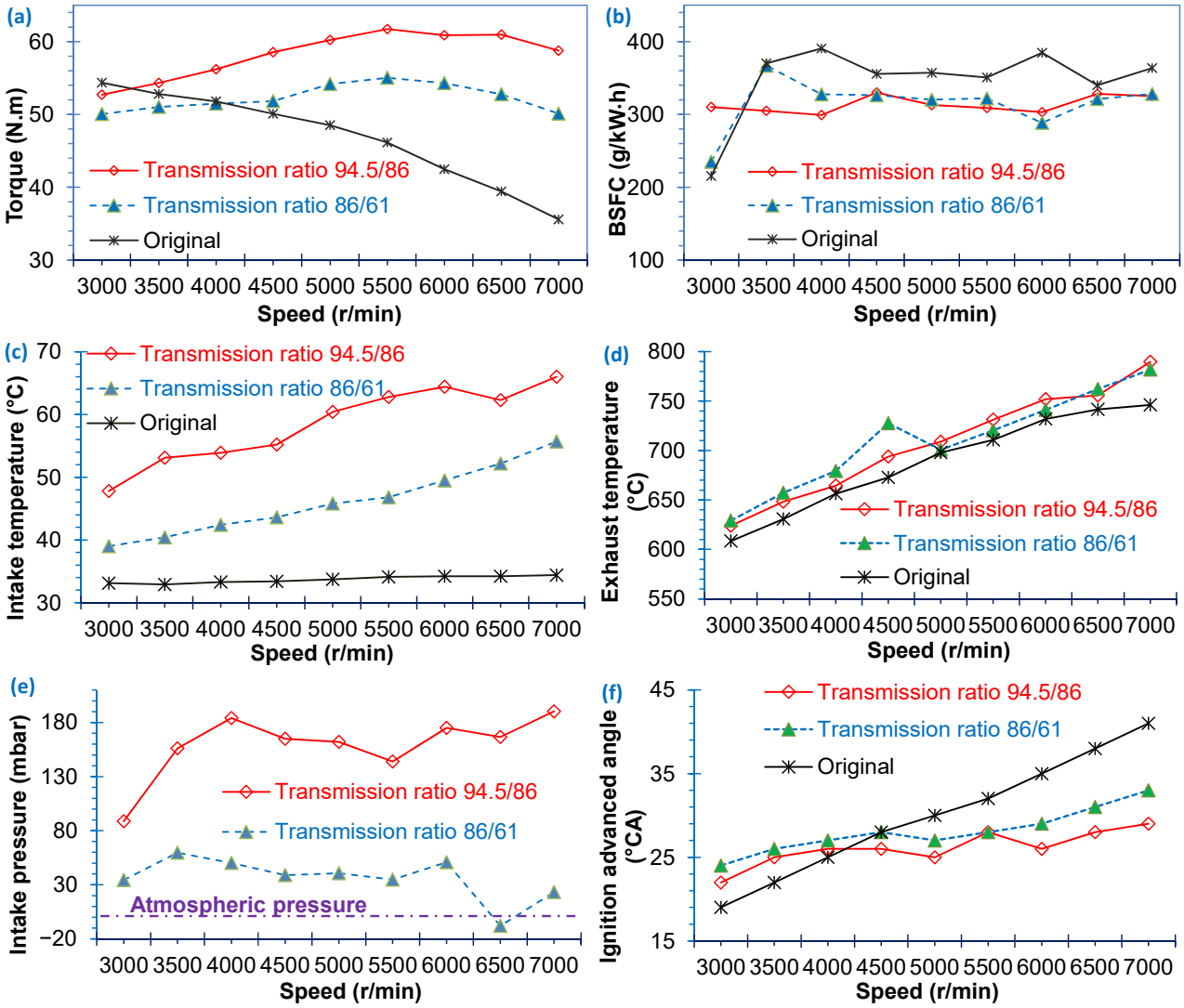


Figure 5. The performances and operating parameters for original and supercharging engine 60% load: (**a**) engine torque, (**b**) brake specific fuel consumption, (**c**) intake temperature, (**d**) exhaust temperature, (**e**) intake pressure, (**f**) ignition advanced angle.

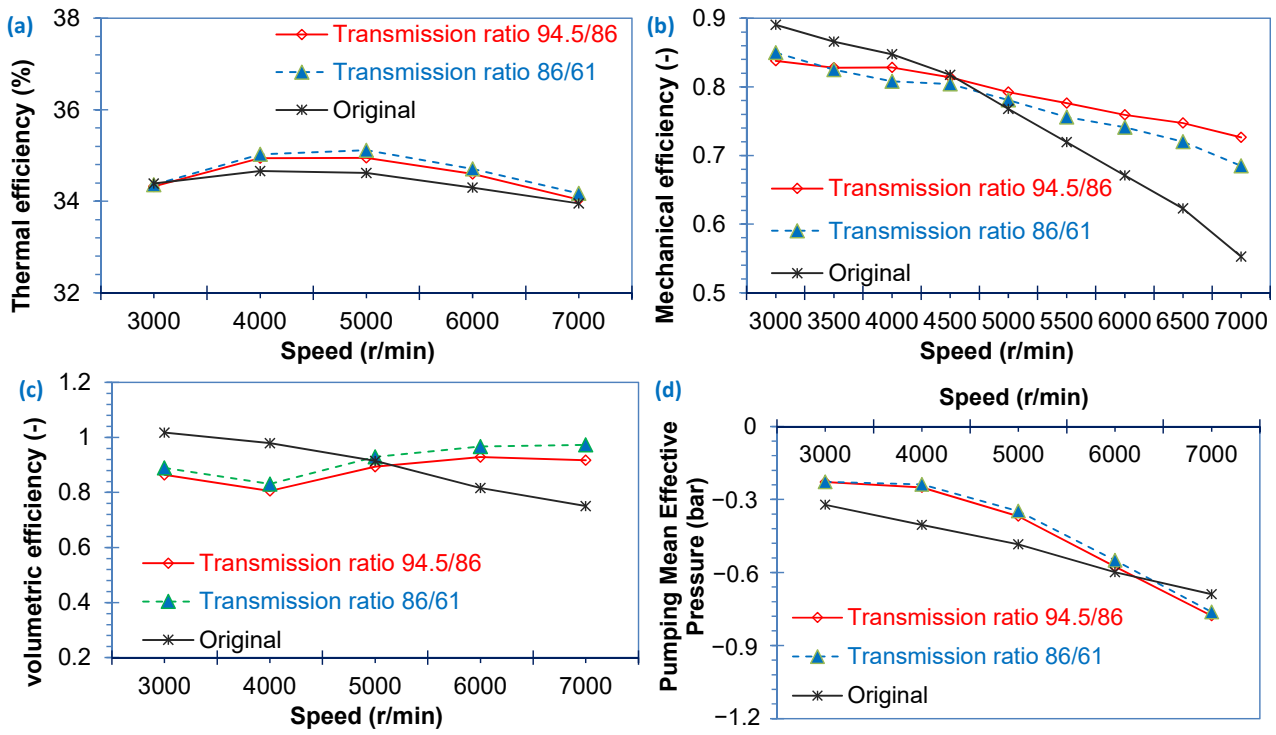


Figure 6. The various efficiencies and pumping loss for original and supercharging engine at 60% engine load: (**a**) thermal efficiency, (**b**) mechanical efficiency, (**c**) intake volumetric efficiency, (**d**) pumping loss (PMEP: pumping mean effective pressure).

The increases in intake air temperature (Figure 5c) and in-cylinder heat release during combustion (the absolute fuel input mass increased after supercharging because of unchanged λ operating mode) resulted in the rise in the exhaust temperature after supercharging (the improvement degree was higher than the 100% load), as shown in Figure 5d. But overall, the 86/61 mode had a slightly higher average exhaust temperature relative to the 94.5/86 mode; this was the compromise result between increased combustion heat release and intake air mass. These results reflected the limit of in-cylinder auto-ignition, thus leading to the adopted ignition advanced angle, as presented in Figure 5f, demonstrating that the transition point (from earlier to later than the original machine) was earlier than that at full load operation (Figure 4f).

Lastly, combining the above results and those in Figure 6, the engine efficiency is discussed. As can be seen in Figure 6a, engine thermal efficiency was up to 34.65% during medium speeds (4000–5000 r/min) for the original engine. And supercharging improved thermal efficiency under the whole speed range, although for other performances, there was a turning point when compared with the original machine. Between the two supercharging modes, the thermal efficiency of the 86/61 mode slightly outperformed the other mode; this was the compromise result among various operating parameters. As mechanical efficiency is concerned (Figure 6b), both supercharging solutions can largely alleviate the decline (due to the increase in force and friction as speed rose [25]) after 4500 r/min; in addition, the 94.5/86 mode had an average of approximately 2% advantage relative to the 86/61 mode, mainly because it outputted greater power that overcame the increase in friction losses. For volumetric efficiency, before 5000 r/min, the original engine already achieved a relatively high volumetric efficiency under 60% load (Figure 6c); supercharging modes lowered the volumetric efficiency, which may be due to the fact that the boosting ratio was not so high to compensate for the negative effect of increased intake temperature (in the current study, the intercooler was absent). But after 5000 r/min, supercharging effectively compensated

for the negative effect of the increase in speed, especially for the 86/61 mode. So, due to an increase in intake pressure, supercharging can decrease pumping loss (Figure 6d), except at the very high speed (7000 r/min). Overall, unlike in the turbocharged engine [26], in which the compressor was driven by exhaust gas and thus the pumping loss significantly decreased (even a positive pumping loop might occur), in the mechanical supercharging operation, the inspired air was almost decoupled from the exhaust gas; therefore, the change in pumping loss was not so obvious.

3.2. Combustion and Emissions

Figures 7–9 give the diagrams of in-cylinder volume-pressure (and the enlarged view of the pumping loop) under 3000 r/min, 5000 r/min and 7000 r/min speeds and 60% load. These phenomena can be discussed from multiple dimensions. At first glance, at all speeds, the cylinder pressures of both turbocharging schemes were significantly higher than those of the original engine, especially near the TDC (top dead center). This also explains the results in Figure 5a, but at 3000 r/min, a slightly higher cylinder pressure cannot compensate for other increases in losses (especially mechanical losses, see Figure 6b). Then, from the viewpoint of speed, the cylinder pressure of the original engine rapidly declined as speed increased, from 3000 r/min to 7000 r/min; the maximum pressure decreased by 19.9%, mainly due to the descent of volumetric efficiency (Figure 6c) because λ was kept constant for a given load; this phenomenon can be reflected from Figure 5a. After supercharging, this phenomenon was improved thanks to the increase in intake volume efficiency as the speed rose (Figure 6c). When compared between the two supercharging modes, the cylinder pressure produced by the "94.5/86" scheme was generally higher than that of the "86/61" scheme (also, the rate of pressure increase was also higher for the former); especially at the low speed of 3000 r/min, the boosting ratio of the latter was not enough to overcome other negative factors (such as the increase in flow loss and/or friction loss). So, at 3000 r/min, the maximal pressure under the 86/61 scheme operation even decreased by 0.2% relative to the original engine; and the 94.5/86 mode only had an increase of 4.4%. While the speed increased to 5000 r/min, the maximal pressure was improved by 16.8% and 27.0%, respectively, by the "86/61" and "94.5/86" schemes. The speed continued to increase to 7000 r/min, which was increased by 35.9% and 51.0%, respectively, by the "86/61" and "94.5/86" schemes. Of course, there are potential reliability issues associated with high-pressure work. The engine was disassembled after the experiment was completed, and no abnormalities or damage was found. But the long-term durability test is still necessary in order to verify reliability.

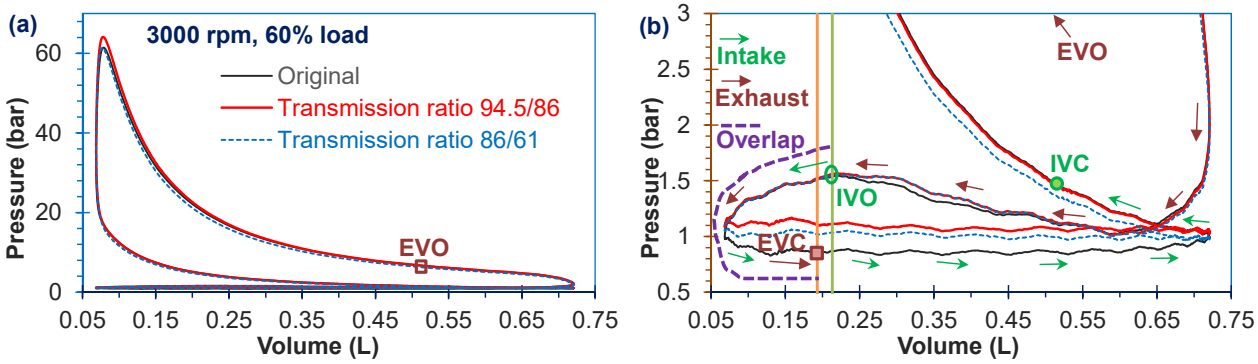


Figure 7. The in-cylinder pressure at 60% engine load and 3000 r/min (**a**), and (**b**) is enlarged view of pumping loop.

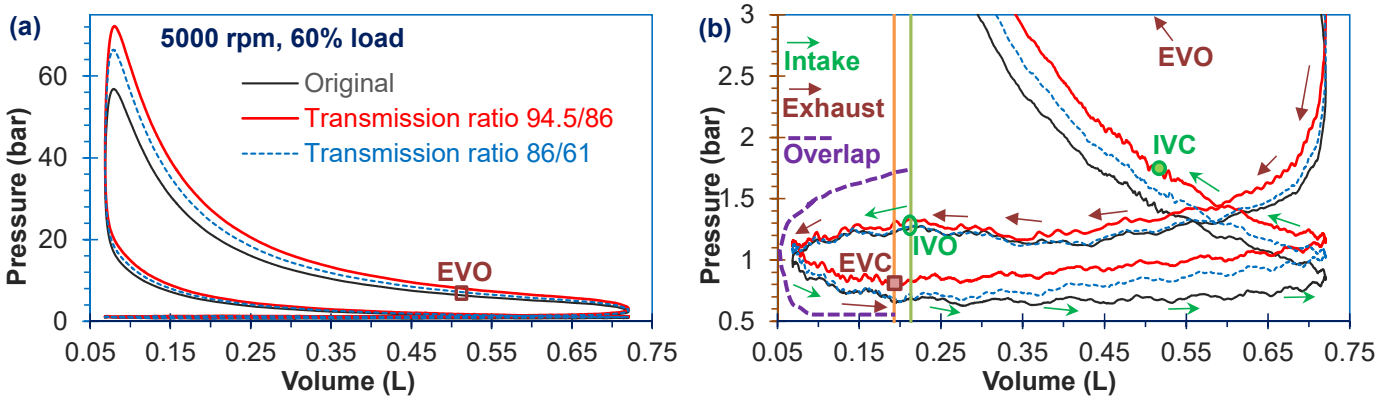


Figure 8. The in-cylinder pressure at 60% engine load and 5000 r/min (**a**), and (**b**) is enlarged view of pumping loop.

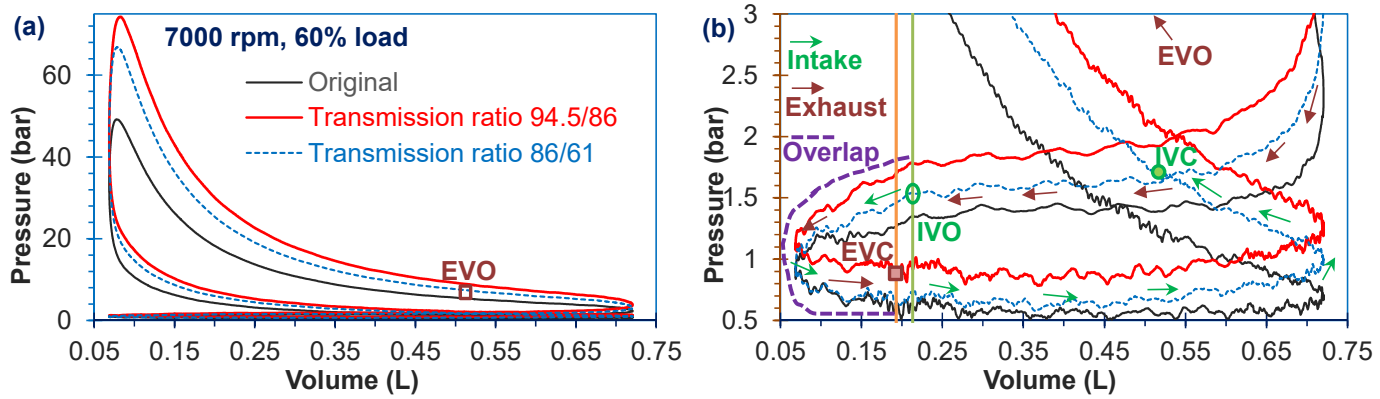


Figure 9. The in-cylinder pressure at 60% engine load and 7000 r/min (**a**), and (**b**) is enlarged view of pumping loop.

Next, for the combined results of Figures 6d, 7b, 8b and 9b, the pumping loss is analyzed. From Figure 6d, except at the very high speed of 7000 r/min, supercharging lowered the pumping loss. From the transient evolution, supercharging decreased pumping loss mainly through improving the intake pressure, while the exhaust pressure changed very weakly at medium and low speeds (Figures 7b and 8b). Although at the high speed of 7000 r/min, the intake pressure was still boosted and enhanced, the exhaust pressure under supercharging operations increased even more intensely due to a more intense combustion process, leading to an extension of the pumping loop (Figure 9b). And on the whole, the pumping loss was very close between the two supercharging schemes.

Next, the combustion parameters are extracted and discussed. Figure 10 provides 50% combustion location and the 10–90% combustion duration. As can be seen, although after supercharging the ignition advanced angle was retarded due to knock constraints at most conditions (Figure 5f), the 50% combustion locations were still earlier than that of the original engine (these phenomena can be also reflected from Figures 7–9), except at the very high speeds of 6000–7000 r/min under the 94.5/86 mode at which ignition advanced angles were very late relative to the original status (Figure 5f). But by making a general observation of the whole combustion process, the combustion durations of the supercharging operations were shorter than the original engine; the 86/61 mode had a 3% average shorter combustion duration than the original operation, and the 94.5/86 mode average shortened the combustion duration by 4.2% relative to the original engine. This demonstrates that because of the higher temperature and turbulence intensity, the combustion rate of supercharging operations can still catch up with the original operation

in the latter part, even if the ignition was delayed; if the ignition was not too late (for example, for the "86/61" scheme operation, the ignition was delayed by no more than 7 degrees relative to "original" at 6500 r/min), the combustion rate was faster than that of the original machine before 50% MFB (Mass Fraction Burned).

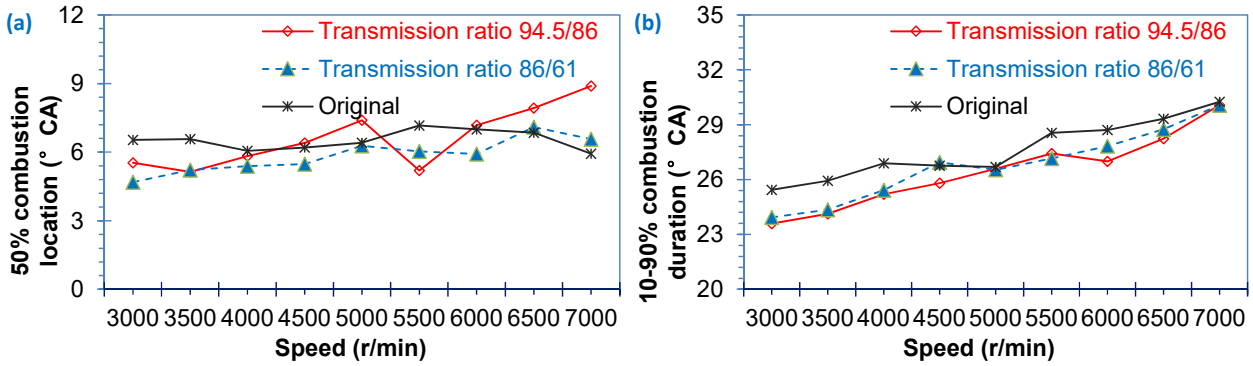


Figure 10. The combustion parameters at 60% engine load: (**a**) 50% combustion location, (**b**) 10–90% combustion duration.

Finally, the engine emissions are summarized. As shown in Figure 11a, raw CO emissions were high for a sport motorcycle engine due to intense combustion (Figures 7–9) and a rich fuel/air mixture. After supercharging, CO emissions were lower during medium speeds (4500–5000 r/min) and higher at both sides relative to original operation. Under rich combustion operations (λ = 0.85 under 60% load), CO generally increased with combustion temperature because a large amount of CO was produced at high temperature, but its oxidation (to CO_2 mainly through reaction CO + OH = CO_2 + H) has been partially suppressed due to oxygen deficiency (including oxygen molecule and oxygen-related free radicals, such as hydroxyl) [24,27]. So, the final production amount of CO is the coordination between its generation and consumption. Due to a higher combustion temperature (which can be indirectly reflected from Figures 7–9), the CO generation under supercharging operation should be higher than that of the original operation during the whole speed range. Except during the 4500–5000 r/min, Figure 11a indeed illustrates this tendency. Behaviors during 4500–5000 r/min can be explained from the aspect of CO consumption; the location of the peak pressure of original and supercharging operation is very close; taking 5000 r/min as an example, from Figure 8a, the peak pressure location is 13.1 °CA, 13.4 °CA and 12.6 °CA, respectively, for the original, 94.5/86 and 86/61 operations, while under supercharging the peak pressure is higher (thus leading to higher temperature). This results in more drastic oxidation of CO (especially for 86/61 operation), thus leading to slightly lower CO emissions, especially for the 86/61 supercharging scheme (its peak pressure appears earlier, which helps to oxidize CO because peak OH radical value often occurs earlier than CO).

For HC (Figure 11b), overall, the emissions decreased as speed increased. The 86/61 supercharging mode lowered the HC emissions at all speeds, while the 94.5/86 mode increased the HC emissions under half of the speed points. Under the 94.5/86 supercharging operation, 4500–5500 r/min is a turning point where HC emission is beyond the original downward trend against speed, while, oppositely, under the 86/61 supercharging scheme, there is a large drop of HC at 4500 r/min. Some reasoning might explain these phenomena: (1) Under the 94.5/86 mode, more fuel/air mixture entered into the crevice due to a specific in-cylinder air motion status, because the crevice effect is the most important source for HC emission [28]. (2) In-cylinder temperature evolution is also a key factor, especially during the post-flame phase. If it is lower than 1500 K, the HC species are hard to oxidize during the post-combustion stage (near the exhaust valve opening moment) [29]. From

Figure 5d (the in-cylinder temperature was not measured, so the exhaust temperature is used to infer the temperature during the post-combustion period), the exhaust temperature of the 86/61 supercharging scheme suddenly increased at 4500 r/min, which explains the sudden drop of HC. (3) Although at 4500 r/min, the exhaust temperature of the 94.5/86 supercharging mode was still higher than that of the original (Figure 5d), from Figure 10b during the 50–90% MFB (Mass Fraction Burned) period, more vigorous combustion of the former generated more intermediate products for the rich fuel/air mixture (λ = 0.85) [30], and the ignition advanced angle was also changed from earlier to later than the original at 4500 r/min (Figure 5f), and thus the temperature in the post-flame period should be lower than the HC oxidation threshold (this aspect will be further investigated by simulation in the future). Lastly, under a constant λ operation, NO_x regeneration is decided by the temperature [31]. So, as expected, the NO_x emissions rose by supercharging under a wide speed range due to higher combustion temperatures (Figure 11c). NO_x decreased as speed increased for the original operation till 5000 r/min, and then, the change was not obvious with speed. While for supercharging modes, NO_x slightly increased with speed change. These phenomena were determined by the combustion process (Figures 7–9).

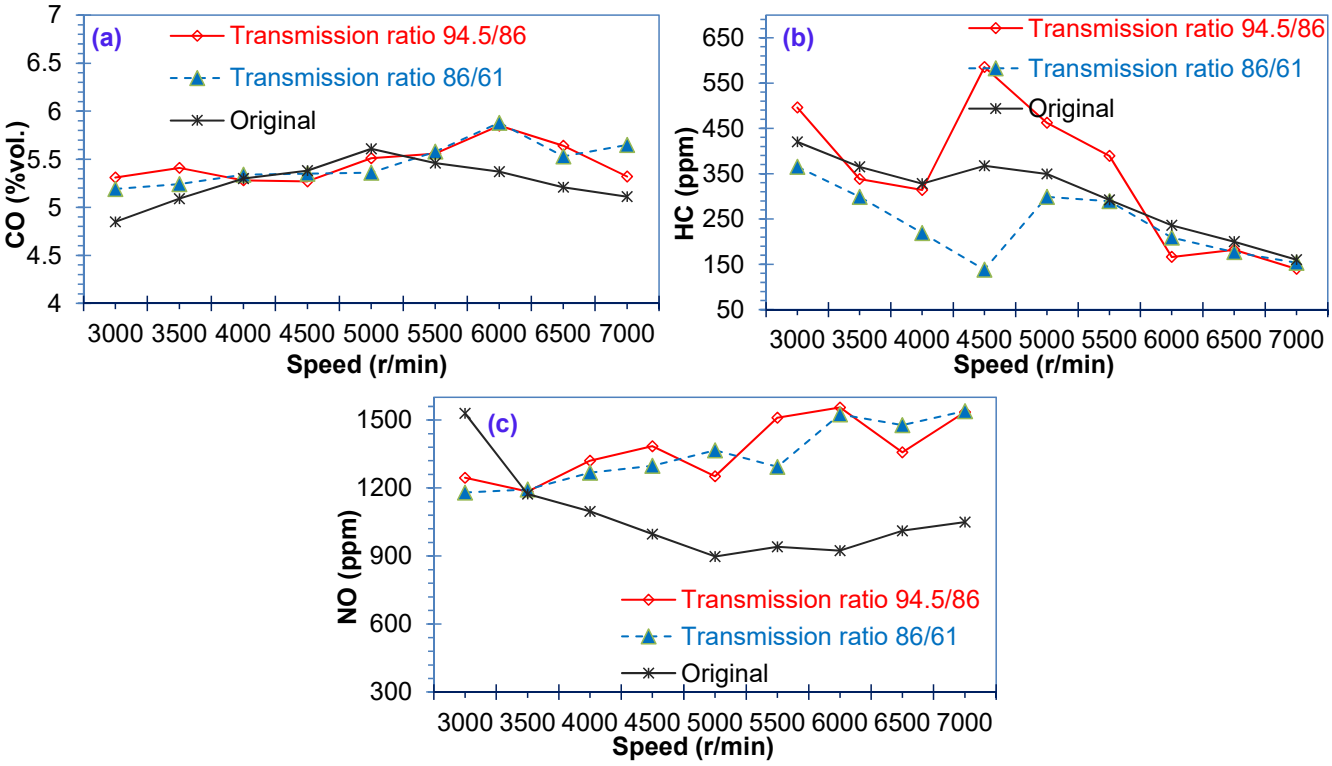


Figure 11. The emissions at 60% engine load: (**a**) CO, (**b**) HC, (**c**) NO.

4. Conclusions

In order to systematically clarify the supercharging effect on performance, combustion and emissions on a high-speed SI engine, in the present study, two supercharging schemes were designed and tested for comparison with the original engine. Some important conclusions are drawn:

(1) When the engine load decreased from full load to 60% load, the boosting effect was more pronounced. Thus, the turning point of the spark advanced angle in the speed range occurred earlier under medium load. This resulted in a considerable reduction (on average by about 9.5% for both supercharging schemes) in BSFC.

(2) At medium engine load, the thermal efficiency of the low speed supercharging mode (engine/compressor speed ratio: 86/61) is almost the same relative to the high-speed mode (engine/compressor speed ratio: 94.5/86), although the latter produces higher engine torque, and it was improved by 0.8% relative to the original engine. This was the compromise result, reflecting various aspects such as mechanical efficiency, intake volumetric efficiency and pump loss.

(3) As engine speed rose, mechanical supercharging overcame the trend of torque decline due to the decrease in intake efficiency, thereby improving the mechanical efficiency and on average decreasing pumping loss by 15%.

(4) Although the ignition timing was delayed due to the knock limit after boosting, the combustion rate recovered in the latter part due to the higher temperature and better combustion organization (stronger in-cylinder air motion), especially for the high-speed supercharging configuration.

(5) As expected, due to the higher temperatures, NO_x emissions increased by 28% in the 94.5/86 supercharging scheme, while almost did not change under low supercharging mode; CO increased by 3.7% in the 94.5/86 ratio supercharging under rich combustion (oxygen was insufficient to completely oxidize CO to CO_2), while the 86/61 supercharging mode almost did not change CO emission; lastly HC increased by 13% and decreased by 21%, respectively, under high and low boosting mode.

In a word, except for emissions, the 94.5/86 supercharging scheme is superior to the 86/61 scheme in other aspects. Considering that this vehicle will be equipped with a three-way catalytic converter, the former is a better trade-off choice. Also, the working process was analyzed in detail, so this study can be expected to provide information and guidance for mechanical supercharging retrofitting of high-speed SI engines.

Author Contributions: Methodology, B.D.; Software, N.Z.; Validation, N.Z. and F.W.; Formal analysis, J.Z.; Data curation, Z.C.; Writing—original draft, G.L.; Supervision, B.D.; Funding acquisition, B.D. All authors have read and agreed to the published version of the manuscript.

Funding: This work was supported by the Program for Scientific Research Start-up Funds of Guangdong Ocean University, China.

Institutional Review Board Statement: Not applicable.

Informed Consent Statement: Not applicable.

Data Availability Statement: The data presented in this study are available on request from the corresponding author.

Conflicts of Interest: The authors declare no conflict of interest.

References

1. Feng, R.H.; Xu, J.H.; Zhao, Z.C.; Dan, Y.; He, J.; Gu, C.; Shu, X.; Xia, X.; Yang, L.; Shen, L. Comparative analysis of energy flow characteristics in a battery-electric heavy-duty tractor-trailer between standard and user driving test cycles. *Energy* **2026**, *335*, 141217. [CrossRef]
2. Wei, H.Q.; Shao, A.F.; Hua, J.X.; Zhou, L.; Feng, D.Q. Effects of applying a Miller cycle with split injection on engine performance and knock resistance in a downsized gasoline engine. *Fuel* **2018**, *214*, 98–107. [CrossRef]
3. Galindo, J.; Climent, H.; de la Morena, J.; González-Domínguez, D.; Guilain, S. Assessment of air management strategies to improve the transient response of advanced gasoline engines operating under high EGR conditions. *Energy* **2023**, *262*, 125586. [CrossRef]
4. Fu, Z.; Xu, X.Z.; Bao, Y.Z.; Zhang, S.K.; Gao, W.Z.; Wu, Y.F.; Wu, W.L. Experimental and simulation study on the effect of supercharging modes on the combustion performance of a hydrogen direct injection engine. *Int. J. Hydrogen Energy* **2026**, *219*, 154033. [CrossRef]

5. Okanishi, N.; Fukutani, I.; Watanabe, E. *Torque Boosting of 4-Stroke Cycle Spark-Lgnition Engine in Low and Middle Engine Speed Ranges by Crankcase-Supercharging*; SAE Technical Paper 840423; SAE International: Warrendale, PA, USA, 1984. [CrossRef] [PubMed]
6. Serrano, J.R.; García, A.; Monsalve-Serrano, J.; Gomez-Vilanova, A.; Martínez-Boggio, S. Performance and emissions of a plug-in hybrid electric vehicle equipped with a two-stroke rodless opposed-piston engine with different boosting conditions. *Fuel* **2026**, *423*, 139226. [CrossRef]
7. Xu, Z.; Pei, J.Z.; Ding, S.T.; Chen, L.F.; Zhong, Z.M.; Yan, H.S.; Du, F.R.; Yang, P.F.; Chang, L.Y.; Zhou, Y. Matching characteristics of high-altitude gas exchange and combined supercharging for two-stroke aircraft engines using sustainable aviation fuel. *Fuel* **2026**, *404*, 136348. [CrossRef]
8. Shen, K.; Xu, Z.S.; Zhu, Z.P.; Yang, L.S. Combined effects of electric supercharger and LP-EGR on performance of turbocharged engine. *Energy* **2022**, *244*, 123176. [CrossRef]
9. Cruz, J.R.S.; López, J.J.; Climent, H.; Gómez-Vilanova, A. Method for turbocharging and supercharging 2-stroke engines, applied to an opposed-piston new concept for hybrid powertrains. *Appl. Energy* **2023**, *351*, 121915. [CrossRef]
10. Gürbüz, H.; Akçay, İ.H. Evaluating the effects of boosting intake-air pressure on the performance and environmental-economic indicators in a hydrogen-fueled SI engine. *Int. J. Hydrogen Energy* **2021**, *46*, 28801–28810. [CrossRef]
11. Oh, H.; Lee, J.; Woo, S.; Park, H. Effect of synergistic engine technologies for 48 V mild hybrid electric vehicles. *Energy Convers. Manag.* **2021**, *244*, 114515. [CrossRef]
12. Shang, H.C.; Zhang, L.; Li, Z.C.; Zhang, Q. Numerical matching of supercharger for gasoline engine based on three-line working condition method. *Case Stud. Therm. Eng.* **2023**, *42*, 102766. [CrossRef]
13. Feng, D.Q.; Wei, H.Q.; Pan, M.Z. Comparative study on combined effects of cooled EGR with intake boosting and variable compression ratios on combustion and emissions improvement in a SI engine. *Appl. Therm. Eng.* **2018**, *131*, 192–200. [CrossRef]
14. Zou, R.; Liu, J.X.; Wang, N.N. Effect of recess shape on combustion performance and knocking characteristics for a downsized gasoline rotary engine. *Appl. Therm. Eng.* **2022**, *214*, 118758. [CrossRef]
15. Wang, R.M.; Qiao, J.H.; Jia, D.D.; Shen, D.Z.; Duan, X.B.; Liu, J.P. Effects of asynchronous late intake valve closing combined with high geometric compression ratio and exhaust gas recirculation on combustion and fuel consumption in a turbocharged SI engine: An experimental study. *Energy* **2024**, *290*, 130058. [CrossRef]
16. Meng, X.L.; Xie, F.X.; Li, X.N.; Han, L.H.; Duan, J.Q.; Gong, Y.F.; Zhou, Y. Study on the effects of intake valve timing and lift on the combustion and emission performance of ethanol, N-butanol, and gasoline engine under stoichiometric combustion and lean burn conditions. *Energy* **2024**, *300*, 131385. [CrossRef]
17. Zhang, Z.J.; Zheng, Z.L. Numerical simulation of the effects of the EGR ratio and ignition timing on a supercharged and high compression ratio hybrid gasoline engine. *Fuel* **2023**, *341*, 127695. [CrossRef]
18. Liu, Z.W.; Zhang, Z.J.; Rao, S.L.; Zheng, Z.L. Study of water injection on suppressing knock in a high compression ratio and supercharged hybrid gasoline engine. *Energy* **2024**, *287*, 129702. [CrossRef]
19. Kolakoti, A.; Koten, H. Effect of supercharging in neat biodiesel fuelled naturally aspirated diesel engine combustion, vibration and emission analysis. *Energy* **2022**, *260*, 125054. [CrossRef]
20. Ma, N.; Gao, Y.L.; Sun, B.G.; Luo, Q.H.; Chen, K.; Bao, L.Z. Co-Optimization of Dual Spark Plug Ignition Timing in a High-Efficiency, Low-Emission Hydrogen-Fueled Aviation Engine. *Aerosp. Sci. Technol.* **2026**, *9*, 112312. [CrossRef]
21. Liu, S.; Lin, Z.L.; Zhang, H.; Fan, Q.H.; Lei, N.; Wang, Z. Experimental study on combustion and emission characteristics of ethanol-gasoline blends in a high compression ratio SI engine. *Energy* **2023**, *274*, 127398. [CrossRef]
22. *GB/T 5363-2008*; Method of Bench Test of Engine for Motorcycles and Mopeds. Standardization Administration of China: Beijing, China, 2008.
23. *GB/T 18297-2024*; Performance Test Code for Road Vehicle Engines. Standardization Administration of China: Beijing, China, 2024.
24. Deng, B.L.; Li, Q.; Chen, Y.Y.; Li, M.; Liu, A.D.; Ran, J.Q.; Xu, Y.; Liu, X.Q.; Fu, J.Q.; Feng, R.H. The effect of air/fuel ratio on the CO and NOx emissions for a twin-spark motorcycle gasoline engine under wide range of operating conditions. *Energy* **2019**, *169*, 1202–1213. [CrossRef]
25. Bobzin, K.; Brögelmann, T. Minimizing Frictional Losses in Crankshaft Bearings of Automobile Powertrain by Diamond-like Carbon Coatings under Elasto-hydrodynamic Lubrication. *Surf. Coat. Technol.* **2016**, *290*, 100–109. [CrossRef]
26. Pirrello, D.; Teodosio, L.; Berni, F. 1D model and rule-based calibration strategy to improve the performance of a turbocharged spark ignition engine over the whole engine map. *Eng. Sci. Technol. Int. J.* **2024**, *60*, 101890. [CrossRef]
27. Shim, E.; Park, H.; Bae, C. Intake air strategy for low HC and CO emissions in dual-fuel (CNG-diesel) premixed charge compression ignition engine. *Appl. Energy* **2018**, *225*, 1068–1077. [CrossRef]
28. Alkidas, A.C. Combustion-chamber crevices: The major source of engine-out hydrocarbon emissions under fully warmed conditions. *Prog. Energy Combust. Sci.* **1999**, *25*, 253–273. [CrossRef]
29. Vera, J.; Ghandhi, J. Investigation of Post-Flame Oxidation of Unburned Hydrocarbons in Small Engines. *SAE Int. J. Engines* **2011**, *4*, 67–81. [CrossRef]

30. Liu, X.Q.; Deng, B.L.; Fu, J.Q.; Xu, Z.X.; Liu, J.P.; Li, M.; Li, Q.; Ma, Z.W.; Feng, R.H. The effect of air/fuel composition on the HC emissions for a twin-spark motorcycle gasoline engine: A wide condition range study. *Chem. Eng. J.* **2019**, *355*, 170–180. [CrossRef]
31. Maiboom, A.; Tauzia, X.; Hétet, J.-F. Influence of EGR unequal distribution from cylinder to cylinder on NOx–PM trade-off of a HSDI automotive Diesel engine. *Appl. Therm. Eng.* **2009**, *29*, 2043–2050. [CrossRef]

Disclaimer/Publisher's Note: The statements, opinions and data contained in all publications are solely those of the individual author(s) and contributor(s) and not of MDPI and/or the editor(s). MDPI and/or the editor(s) disclaim responsibility for any injury to people or property resulting from any ideas, methods, instructions or products referred to in the content.